Pramana – J. Phys. (2018) 91:86
https://doi.org/10.1007/s12043-018-1653-7

Clusterisation and isospin effects in heavy-ion collisions at intermediate energies

RAJNI MITTAL and YOGESH K VERMANI*

Department of Physics, Sri Guru Granth Sahib World University, Fatehgarh Sahib 140 406, India
*Corresponding author. E-mail: yugs80@gmail.com

MS received 9 October 2017; revised 15 December 2017; accepted 4 May 2018; published online 9 October 2018

Abstract. We study the multifragmentation phenomenon in heavy-ion collisions by varying the spatial constraint criterion in minimum spanning tree (MST) clusterisation procedure. Within the framework of isospin-dependent quantum molecular dynamics (IQMD) model, the role of isospin-dependent spatial constraint, i.e. iso-MST version, is investigated on different fragment observables in various isobaric pair of reaction systems varying in the entrance channel isospin (N/Z) content. The fragment observables such as persistence, gain, average yield of free nucleons, light and intermediate mass fragments are slightly sensitive to the isospin-dependent spatial constraint criterion particularly in heavier reaction systems. For a given isobaric pair of reaction systems, the fragment production, however, remains indifferent to isospin content of the colliding nuclei.

Keywords. Heavy-ion collisions; isospin-dependent quantum molecular dynamics model; minimum spanning tree algorithm; multifragmentation.

PACS Nos 24.10.Cn; 24.10.Lx; 25.70.Mn; 25.70.Pq

1. Introduction

The study of heavy-ion (HI) collisions at intermediate and higher incident energies is mainly concerned with the properties of hot and dense nuclear matter. The production of free nucleons, light mass fragments (LMFs) ($2 \leq A \leq 4$) and intermediate mass fragments (IMFs) in HI collisions can provide useful information about the nuclear matter equation of state (EoS) and non-equilibrium features of reaction dynamics [1–5]. On the experimental front, the systematic study of symmetric HI reactions has been reported by FOPI Collaboration [2,6,7]. The production of IMFs and degree of thermalisation achieved in HI collisions were some of the key aspects in these FOPI experiments [2,3,8]. Further, the mechanism behind the light and intermediate mass cluster production is largely studied due to the possible signature of liquid–gas phase transition and bimodality in the nuclear system [5,9]. The multifragment production following the collisions of ^{197}Au on ^{197}Au and other heavy nuclei at relativistic bombarding energies has been studied on the ALADiN forward spectrometer at GSI, Darmstadt [10–12]. These experimental studies emphasised the remarkable universality behaviour in the spectator matter fragmentation irrespective of bombarding energy and mass of the target nucleus. The observed yields of IMFs were, however, underpredicted by the quantum molecular dynamics (QMD) simulations [10,12,13]. These simulations employed the conventional minimum spanning tree (MST) procedure to clusterise the phase space of nucleons [14,15]. In the simplest MST algorithm, we define two nucleons as a member of a complex fragment if the relative distance between their centroids in the configuration space satisfies the relation $|\mathbf{r_i} - \mathbf{r_j}| \leq R_\circ$. Here $\mathbf{r_i}$ ($\mathbf{r_j}$) is the centroid of the ith (jth) nucleon in the configuration space with parameter $R_\circ$ known as 'coalescence radius' [14]. Many attempts have been made in the past few decades to improvise upon the conventional clusterisation algorithm. One such attempt was early cluster recognition algorithm (ECPA). This algorithm identifies the fragmentation pattern that gives the highest binding energy [16]. Later on, a faster cluster recognition algorithm dubbed as simulated annealing clusterisation algorithm (SACA) was developed by Puri and collaborators [17–20]. This clusterisation approach was based on the minimisation of the fragment's total energy using a metropolis algorithm. This clustering procedure

would eventually yield the most bound configuration (MBC) quite earlier when the nuclear matter is still hot and non-equilibrated. Later on, further refinements to MST procedure and SACA were suggested [21]. In these refinements, procedure the fragments filtered through the MST method were subjected to a realistic binding energy check based on the Bethe–Weizsäcker mass (BWM) formula [21]. These secondary clusterisation algorithms were helpful in understanding the mechanism behind the spectator matter fragmentation and yields of IMFs. These microscopic clusterisation approaches, however, do not take into account the isospin of the interacting nucleons to predict the final cluster yields.

In this paper, we focus on the fragmentation process and analysis of the concerned observables in isobaric pairs of symmetric reaction systems selected over a wide range of system masses. The choice of isobaric colliding systems with different N/Z values in the entrance channel allows to infer isospin effects on the fragmentation process properly. In an isospin-dependent transport theory, the two essential ingredients are the symmetry potential of the mean field and the isospin-dependent in-medium n–n cross-section [22,23]. These ingredients are observed to affect the HI collision dynamics significantly [24–31]. For instance, these isospin-dependent parameters influence the production of LMFs, multiplicities of IMFs [22,23,31], quadrupole of a single-particle momentum distribution Q_{zz} in the neutron-rich and neutron-deficient systems [22]. The cluster production is a complex phenomenon which depends on the entrance channel parameters (viz. mass of the colliding nuclei, bombarding energy and colliding geometry). For instance, in the central collisions, the colliding nuclei exhibit fireball picture with the nuclear fragments showing exponential charge distribution [3]. In peripheral geometries, on the other hand, the spectator matter is relatively uncompressed and cold. The spectator matter undergoes complete equilibration as indicated by the universality in the production of IMFs [11]. The importance of isospin-dependent spatial constraints in the identification of stable clusters is not much explored in the past. Recently, Zhang *et al* [32] used the optimum value of spatial constraint $R_\circ$ in the MST method depending on the isospin of the interacting nucleons. The cluster recognition method so modified was observed to enhance the production of neutron-rich isotopes at midrapidity.

In §2, brief details of the isospin-dependent quantum molecular dynamics (IQMD) model along with the secondary MST algorithm and its isospin-dependent versions are discussed. The model calculations as well as comparison with the experimental data are given in §3 and finally conclusion is given in §4.

2. The IQMD model

The nucleon coordinates for the target and projectile nuclei in the configuration and momentum space are generated within the framework of IQMD model [14,15]. The IQMD model has been used successfully for the analysis of a large number of observables from low to relativistic energies. The isospin degree of freedom enters into the calculations via symmetry potential, cross-sections and Coulomb interactions [15]. The details about the elastic and inelastic cross-sections for proton–proton and neutron–neutron collisions can be found in [15]. In this model, the baryons are represented by Gaussian wave packets in the coordinate and momentum space:

$$f_i(\mathbf{r},\mathbf{p},t) = \frac{1}{\pi^2\hbar^2}\cdot \mathrm{e}^{\frac{-(\mathbf{r}-\mathbf{r_i}(t))^2}{2L}}\cdot \mathrm{e}^{-(\mathbf{p}-\mathbf{p_i}(t))^2\frac{2L}{\hbar^2}}. \tag{1}$$

Here, the Gaussian width L is a free parameter and is linked with the interaction range of the particle. For the heavier systems, such as ^{197}Au $+^{197}$Au, we have taken the standard value of L ($= 8.66$ fm^2) while for lighter ^{40}Ca $+^{40}$Ca system we take $L = 4.33$ fm^2. The choice of the wave packet width L has to be adjusted so as to ensure stable density profiles of the target and projectile nuclei [15]. Nucleons are initialised in a sphere with radius $R = 1.12A^{1/3}$ fm in accordance with the droplet model [33], so as to give Fermi-type distribution of neutrons and protons. The initial momenta are randomly chosen between 0 and Fermi momentum ($\mathbf{P}_\mathrm{F}$). The nucleons of the target and projectile nuclei interact via two- and three-body Skyrme forces, Yukawa, Coulomb and symmetry potentials and momentum-dependent interactions as an additional option:

$$V^{ij} = V^{ij}_{\mathrm{Sky}} + V^{ij}_{\mathrm{Yuk}} + V^{ij}_{\mathrm{Coul}} + V^{ij}_{\mathrm{Sym}} + V^{ij}_{\mathrm{MDI}}. \tag{2}$$

Parameters used for these interaction terms can be found in [14,15]. The centroids of these wave packets are propagated using Hamilton's equations of motion:

$$\dot{\mathbf{r}}_\mathbf{i} = \frac{\mathrm{d}H}{\mathrm{d}\mathbf{p_i}};\quad \dot{\mathbf{p}}_\mathbf{i} = -\frac{\mathrm{d}H}{\mathrm{d}\mathbf{r_i}}, \tag{3}$$

where the total Hamiltonian H reads as

$$\begin{aligned} H &= T + V \\ &= \sum_i \frac{\mathbf{p_i}^2}{2m_i} + \sum_i \sum_{j>i} \int f_i(\mathbf{r},\mathbf{p},t) V^{ij} \\ &\quad \times f_j(\mathbf{r}',\mathbf{p}',t)\,\mathrm{d}\mathbf{r}\,\mathrm{d}\mathbf{r}'\mathrm{d}\mathbf{p}\,\mathrm{d}\mathbf{p}'. \end{aligned} \tag{4}$$

The inclusion of the symmetry potential $V_{\rm sym}$ allows for isospin treatment for distribution of protons and neutrons:

$$V_{\rm sym} = t_6 \frac{1}{\varrho_0} \tau_i \tau_j \delta(\mathbf{r_i} - \mathbf{r_j}). \tag{5}$$

Here τ_i, τ_j are the third components of isospin degree of freedom of the ith and jth baryons, respectively. τ_i equals $+1$ for protons and -1 for neutrons. In addition to the symmetry potential, the repulsive Coulomb interaction takes into account the explicit charges of nucleons:

$$V_{\rm Coul} = \sum_i \sum_{j>i} \frac{Z_i Z_j e^2}{|\mathbf{r_i} - \mathbf{r_j}|}. \tag{6}$$

Here, Z_i and Z_j denote the charges of the ith and jth baryons, respectively. The two nucleons propagating in the phase space are supposed to undergo a stochastic binary collision if the relative distance between their centroids fulfils

$$|\mathbf{r_i} - \mathbf{r_j}| \leq \sqrt{\frac{\sigma_{\rm tot}}{\pi}}, \quad \sigma_{\rm tot} = \sigma(\sqrt{s}, \text{type}). \tag{7}$$

Here, the 'type' denotes the ingoing collision partners (N–N, N–Δ, N–π, ...). In addition, to prevent the nucleons from being in an overpopulated state, the phase space around the scattering partners is checked by taking into account the Pauli blocking [15]. It is worth mentioning that recent studies on collective flow [34–37] have suggested a need for reduced isospin-dependent cross-section. In another contribution [25], it was suggested for the demand of a reduced isospin-dependent cross-section ($\sigma = 0.88\sigma_{\rm nn}$) to better explain the experimental data. For the present analysis, a soft equation of state along with the reduced isospin-dependent cross-section ($\sigma = 0.8\sigma_{\rm nn}$) has been employed. The time evolution of HI reaction is followed up to 400 fm/c when the nuclear fragments are relatively stable and cold. The phase space generated using the IQMD model is clusterised using the secondary clusterisation algorithm which is described in the following subsection.

2.1 *Secondary clusterisation algorithm*

The simplest algorithm for cluster recognition is based on the coalescence phenomenon in which the two interacting nucleons are assumed to be members of a complex fragment if their relative distance in the configuration space is smaller than $R_\circ$. This method is commonly known as the MST procedure [14,38]. The parameter $R_\circ$ is a free parameter which is usually chosen in the range 3–6 fm. It may be mentioned that the final fragmentation pattern does not depend sensitively on the correlation length $R_\circ$ because, after 400 fm/c the nucleons bound in different clusters are far apart in the configuration space.

For the present analysis, we aim to infer the role of introducing isospin-dependent spatial constraint criterion in the MST algorithm. We employ two versions of isospin-dependent MST (iso-MST) algorithm by varying the spatial correlation distance $R_\circ$ for different kinds of nucleons. One version uses $R_{\rm nn,np} = 6$ fm and $R_{\rm pp} = 3$ fm, while the other version uses narrower constraint, i.e. $R_{\rm nn,np} = 4.5$ fm and $R_{\rm pp} = 3.2$ fm, where p and n stand for proton and neutron. The larger value of $R_{\rm nn}$ (or $R_{\rm np}$) is also consistent with the properties of neutron-rich nuclei, viz. neutron skin thickness and neutron halo effects.

3. Results and discussion

In order to understand the effect of varying spatial constraint criteria in the cluster identification algorithm, we simulated HI reactions involving pairs of isobaric reaction systems having different N/Z values but the same system size $A_{\rm tot}$. An important concern in the study of multifragmentation is the stability of fragments formed in HI collisions. The persistence coefficient is an important fragment observable to understand the general behaviour of fragmentation process with time [17]. The persistence coefficient quantifies the change in nucleon content of the fragment between two successive time steps [17,39,40]. Let N_C be the number of nucleons in cluster C at time t. The number of nucleon pairs in cluster C at that time t is defined as $b_C(t) = 0.5N_C(N_C - 1)$. After certain time interval Δt, some nucleons have left the cluster C and are part of other clusters or are singles. Let N_{C_A} be the number of nucleons which have been part of cluster C at time t and are at $t + \Delta t$ in the cluster A. We define $a_C(t + \Delta t) = \sum_A 0.5N_{C_A}(N_{C_A} - 1)$, where the sum is over all clusters A present at time $(t + \Delta t)$. The persistence coefficient for the cluster C is then defined as [39,40]

$$P_C\left(t + \frac{\Delta t}{2}\right) = a_C\left(t + \frac{\Delta t}{2}\right) \Big/ b_C(t). \tag{8}$$

The average persistence coefficient P for an ensemble of clusters is then defined as

$$P\left(t + \frac{\Delta t}{2}\right) = \left\langle \frac{1}{N_t} \sum_{C=1}^{N_t} P_C\left(t + \frac{\Delta t}{2}\right) \right\rangle, \tag{9}$$

where N_t is the number of fragments present at time t in a single simulation. The quantity is then averaged over large number of IQMD simulations. If the fragment does not emit a nucleon between two time steps, the persistence coefficient equals one. On the other hand,

if a fragment disintegrates completely, the persistence coefficient will be zero. Another term closely associated with the persistence coefficient is the gain factor. The gain represents the percentage of nucleons that a fragment has swallowed between two consecutive time steps or whether the interactions among the fragments have ceased or not. It represents the per cent gain of nucleons for a given cluster between the two time steps. Let N_C be the number of nucleons in cluster C at time t. Let N_{C_A} be the number of clusters which have been part of the cluster C at time t and are at $t + \Delta t$ in cluster A. The gain factor at later time $(t + \Delta t)$ is, therefore, defined as

$$\text{Gain}\left(t + \frac{\Delta t}{2}\right) = \eta \times \frac{\sum_A (N_A - N_{C_A})}{N_C}. \tag{10}$$

We take $\eta = 0, 0.5$ and 1 if $N_{C_A} < 0.5N_A$, $N_{C_A} = 0.5N_A$ if $N_{C_A} > 0.5N_A$, respectively. The gain factor of the fragments approaches zero when the distance between the nucleons is higher, indicating that the interactions among the fragments have been ceased at the freeze-out stage.

In figure 1, we display the time evolution of persistence coefficient and gain factor for IMFs ($5 \le A \le A_{\text{tot}}/6$) formed in semicentral collisions ($b/b_{\max} = 0.2$) of ^{40}Ca + ^{40}Ca ($N/Z = 1$) and ^{40}Ar +^{40}Ar ($N/Z = 1.22$) at an incident energy of 150 MeV/nucleon. From this figure, we find that the persistence coefficient is close to unity at freeze-out stages indicating the formation of stable fragments. Interestingly, the persistence coefficient at the end of the reaction approaches the same value for both the isobaric reaction systems. The final persistence and gain values in both the reaction systems are also rather insensitive towards different criteria of spatial constraint employed in the iso-MST algorithm. The time evolution of the size of heaviest fragment $\langle A^{\max} \rangle$, multiplicity of free nucleons, LMFs and IMFs is shown in figure 2 for the same reactions as studied in figure 1. As expected, the average size of the heaviest fragment and yields of various fragments obtained at the freeze-out stage are not sensitive to the varying ranges of spatial constraints used in the MST and iso-MST versions.

The size of the heaviest fragment and mean multiplicity of different fragments obtained in these two isobaric reaction systems are further compared at different colliding geometries to look for the possible influence of isospin content (i.e. N/Z values) of colliding

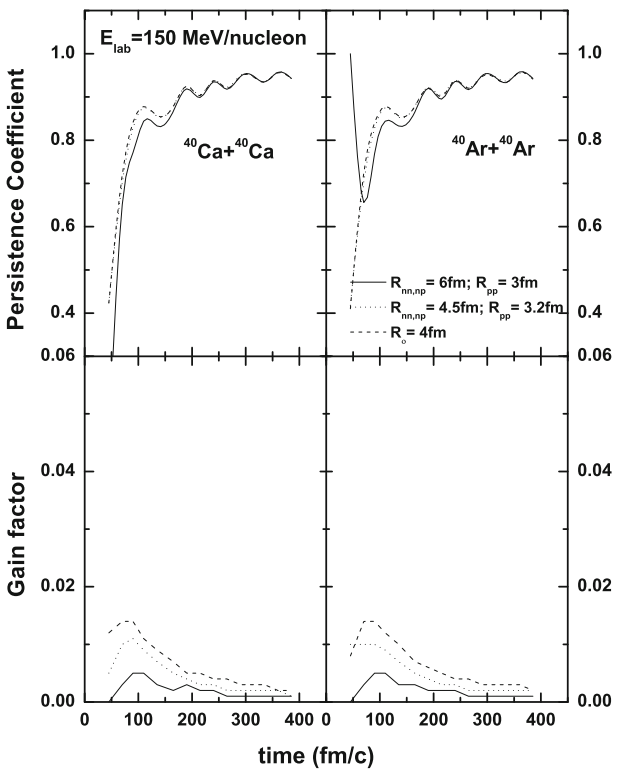

Figure 1. The persistence coefficient and the gain factor for IMFs as a function of time for the set of isobaric reaction systems ^{40}Ca + ^{40}Ca (l.h.s.) and ^{40}Ar +^{40}Ar (r.h.s.) at 150 MeV/nucleon incident energy and at reduced impact parameter $b/b_{\max} = 0.2$.

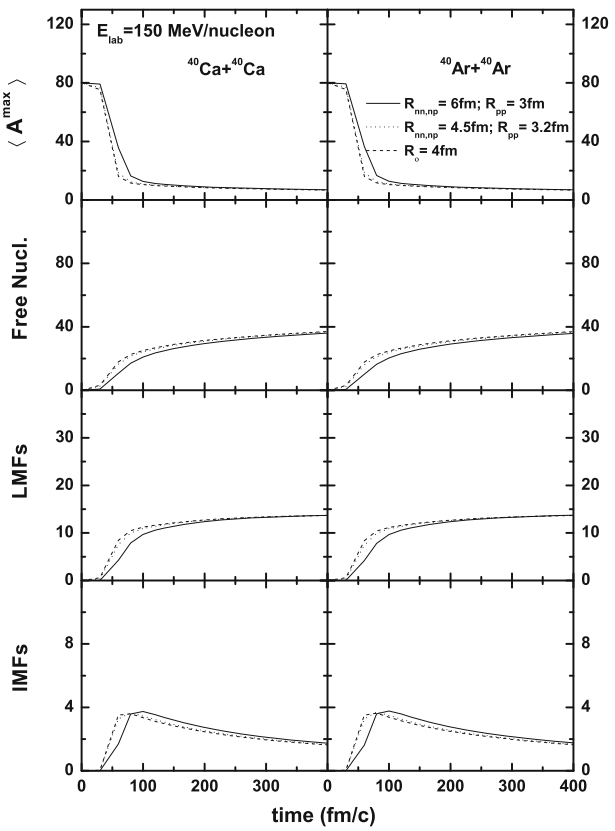

Figure 2. The time evolution of size of the heaviest fragment $\langle A^{\max} \rangle$, multiplicity of free nucleons, light mass fragments (LMFs) and intermediate mass fragment (IMFs) for the same set of reactions as studied in figure 1.

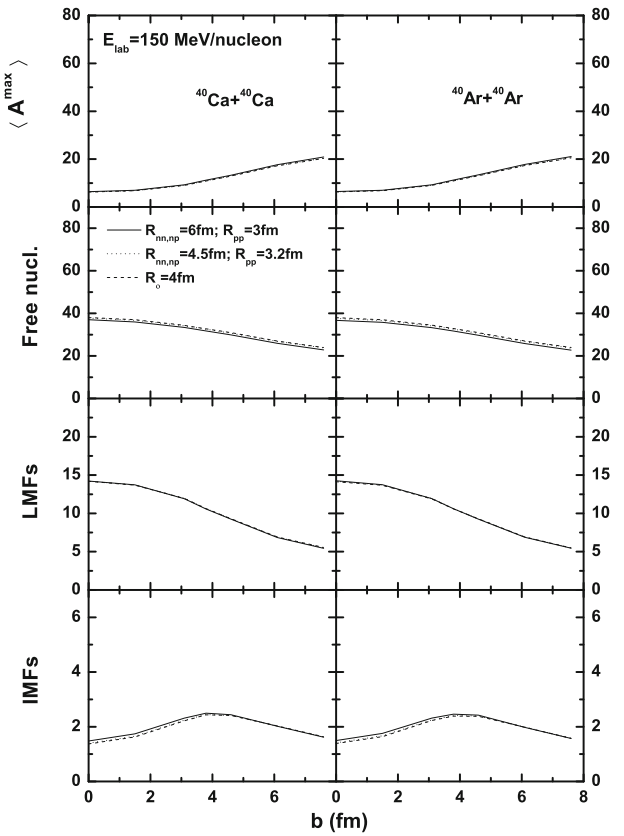

Figure 3. The impact parameter dependence of the size of the heaviest fragment $\langle A^{\max}\rangle$, and the multiplicities of various fragment species in ^{40}Ca+^{40}Ca (l.h.s.) and ^{40}Ar+^{40}Ar (r.h.s.) collisions at 150 MeV/nucleon.

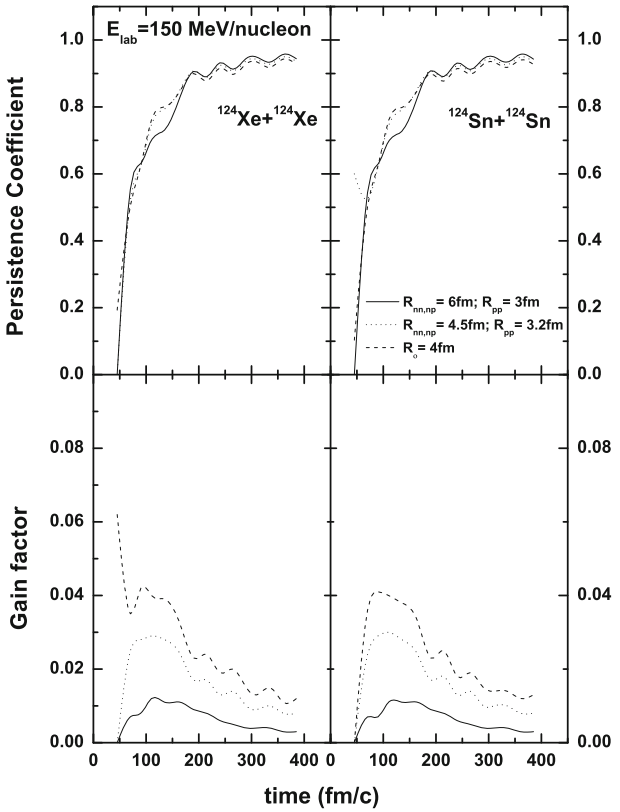

Figure 4. The persistence coefficient and the gain factor for IMFs as a function of time for the set of isobaric reaction systems ^{124}Xe+^{124}Xe (l.h.s.) and ^{124}Sn +^{124}Sn (r.h.s.) at an incident energy of 150 MeV/nucleon at reduced impact parameter $b/b_{\max} = 0.2$.

nuclei. Figure 3 shows the impact parameter-dependent yields of various fragments in isobaric reaction systems of ^{40}Ca +^{40}Ca and ^{40}Ar + ^{40}Ar at an incident energy of 150 MeV/nucleon. One can find well-known trends for the size of the heaviest fragment $\langle A^{\max}\rangle$, mean multiplicities of free nucleons, LMFs and IMFs as a function of impact parameter. The mean IMF multiplicity is marked by the 'rise and fall' behaviour due to the onset of vapourisation at smaller impact parameters. The final fragment yields obtained in both the isobaric reaction systems are identical irrespective of the isospin content of the colliding nuclei. It is worth seeing again that at all the colliding geometries, these fragment observables are independent of the isospin-dependent spatial constraint criterion used in the MST procedure. In other words, the iso-MST versions predict almost the same yields as obtained with the conventional MST procedure. Figure 4 displays the persistence coefficient and gain quantities calculated for heavier reaction systems of ^{124}Xe +^{124}Xe ($N/Z = 1.30$) and ^{124}Sn + ^{124}Sn ($N/Z = 1.48$) having the same system size. The final stage persistence and gain approach the same values for both the reaction systems, although the colliding nuclei in the two systems bear different N/Z ratios. The persistence coefficient obtained using the iso-MST algorithm with $R_{\rm nn,np} = 6$ fm and $R_{\rm pp} = 3$ fm has slightly higher value than that obtained with $R_{\rm nn,np} = 4.5$ fm, $R_{\rm pp} = 3.2$ fm. Overall, the spatial constraint condition used is found to have nearly no effect on the calculated persistent and gain values. We further plot in figure 5, the size of the heaviest fragment and multiplicity of various fragment species predicted for the same reactions as studied in figure 4. The IQMD model simulations of these isobaric reaction systems lead to similar yield of fragments at freeze-out stage. In other words, the yields remaining insensitive to the isospin content of a reaction system is clearly visible in heavier systems as well.

However, one main difference is that the production of free nucleons, light mass clusters and intermediate mass fragments are slightly influenced by the spatial constraint criterion employed. The iso-MST algorithm with $R_{\rm nn,np} = 6$ fm, $R_{\rm pp} = 3$ fm predicts slightly higher yield of IMFs compared to the other clusterisation versions. From this analysis, one can see that the final fragment multiplicities are not much affected

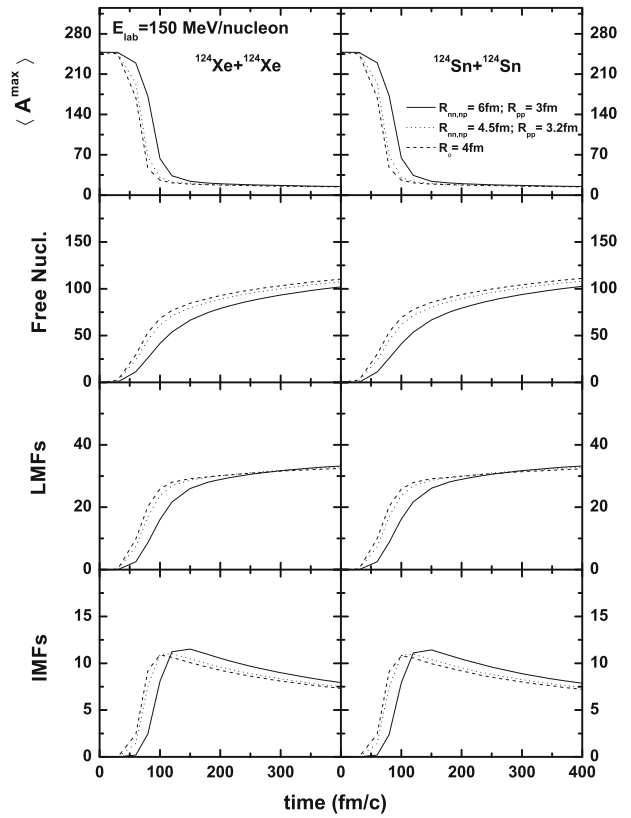

Figure 5. The time evolution of size of the heaviest fragment $\langle A^{\max} \rangle$, multiplicity of free nucleons, light mass fragments (LMFs) and intermediate mass fragment (IMFs) for the same set of reactions as studied in figure 4.

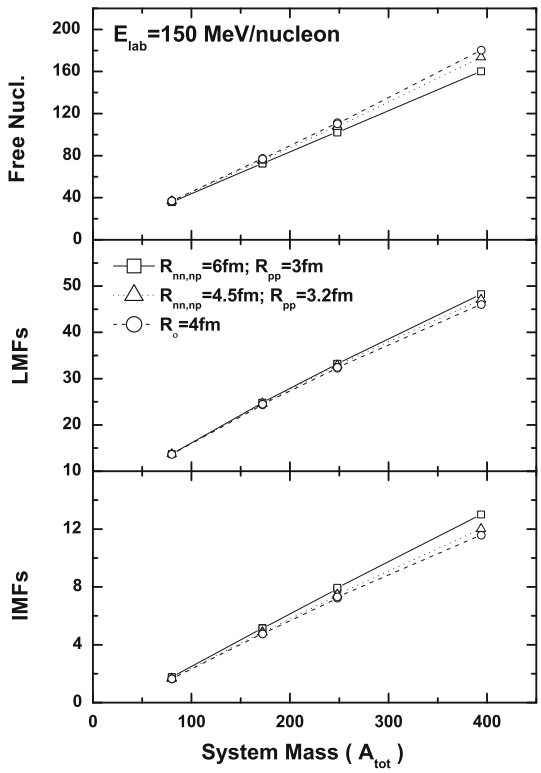

Figure 6. Multiplicity of free nucleons, light mass fragments (LMFs) and intermediate mass fragment (IMFs) calculated as a function of system size $A_{\rm tot}$. Model calculations are shown for different reaction systems: ^{40}Ca $+^{40}$Ca and ^{40}Ar $+^{40}$Ar ($A_{\rm tot} = 80$); ^{86}Kr $+^{86}$Kr and ^{86}Sr $+^{86}$Sr ($A_{\rm tot} = 172$); ^{124}Xe $+^{124}$Xe and ^{124}Sn $+^{124}$Sn ($A_{\rm tot} = 248$); and ^{197}Au $+^{197}$Au ($A_{\rm tot} = 394$) at $E_{\rm lab} = 150$ MeV/nucleon and at the reduced impact parameter $b/b_{\max} = 0.2$.

by the isospin content of the colliding nuclei. To understand the effect of varying spatial constraint in cluster recognition over a wide range of system masses, we calculated the final-stage multiplicities of free nucleons, light mass and intermediate mass fragments as a function of system size $A_{\rm tot}$ ($= A_T + A_P$). In figure 6, we show the multiplicities calculated using different spatial constraint criteria employed in the clusterisation algorithm. We display here the fragment yields obtained in the isobaric reaction systems ^{40}Ca $+$ ^{40}Ca and ^{40}Ar$+^{40}$Ar ($A_{\rm tot} = 80$); ^{86}Kr$+^{86}$Kr and ^{86}Sr$+^{86}$Sr ($A_{\rm tot} = 172$); ^{124}Xe $+$ ^{124}Xe and ^{124}Sn $+$ ^{124}Sn ($A_{\rm tot} = 248$). As we move from lighter systems to heavier ones, the predicted fragment yields remain the same for isobaric pair of reactions with fixed system size $A_{\rm tot}$. It is argued that as far as isospin-dependent cluster recognition is concerned, the fragment yields are only slightly sensitive to the spatial constraint condition. Also, shown in the figure are the multiplicities of various fragments obtained in ^{197}Au $+^{197}$Au reaction with the system size $A_{\rm tot} = 394$. Even in the case of the heaviest ^{197}Au $+^{197}$Au system, the multiplicity fluctuations of fragments arising due to spatial constraint condition are negligibly small and the average dispersion is well within 8–9%. One can conclude that the effect of isospin-dependent spatial constraint condition on fragment observables is hardly pronounced.

4. Conclusion

In summary, we have reported the microscopic study of the role of isospin-dependent spatial constraint used in cluster recognition on various fragment observables. This analysis is carried out by simulating isobaric pairs of symmetric reaction systems. The calculations performed within the framework of the IQMD model predicted identical fragment yields for isobaric reaction systems irrespective of their isospin content (or N/Z ratios).

For a given total mass of the system $A_{\rm tot}$, the fragment production is found to be identical in isobaric pair of reactions independent of their isospin content. It is argued that as far as heavier systems are concerned,

the sensitivity of fragment yields to the choice of spatial constraint condition is only meagerly visible. Based on these observations, it is the natural outcome that the cluster production is not affected by isospin dependence of spatial constraint condition employed in the clusterisation algorithm.

Acknowledgements

The authors thank Prof. R K Puri at Panjab University, Chandigarh, for providing access to the IQMD transport code for the present work. This work was supported by the research grant from the Department of Science and Technology (DST), Government of India vide Grant No. SR/WOS-A/PS-13/2014.

References

[1] J P Alard *et al*, *Phys. Rev. Lett.* **69**, 889 (1992)
[2] S C Jeong *et al*, *Phys. Rev. Lett.* **72**, 3468 (1994)
[3] W Reisdorf *et al*, *Nucl. Phys. A* **612**, 493 (1997)
[4] M A Lisa *et al*, *Phys. Rev. Lett.* **75**, 2662 (1995)
[5] M D'Agostino *et al*, *Nucl. Phys. A* **749**, 55c (2005)
[6] C Kuhn *et al*, *Phys. Rev. C* **48**, 1232 (1993)
[7] M Petrovici *et al*, *Phys. Rev. Lett.* **74**, 5001 (1995)
[8] F Rami *et al*, *Phys. Rev. Lett.* **84**, 1120 (2000)
[9] A Le Fèvre and J Aichelin, *Phys. Rev. Lett.* **100**, 042701 (2008)
[10] M Begemann-Blaich *et al*, *Prog. Part. Nucl. Phys.* **30**, 181 (1993)
[11] A Schüttauf *et al*, *Nucl. Phys. A* **607**, 457 (1996)
[12] C A Ogilvie *et al*, *Phys. Rev. Lett.* **67**, 1214 (1991)
[13] M B Tsang *et al*, *Phys. Rev. Lett.* **71**, 1502 (1993)
[14] J Aichelin, *Phys. Rep.* **202**, 233 (1991)
[15] Ch Hartnack, R K Puri, J Aichelin, J Konopka, S A Bass, H Stöcker and W Greiner, *Eur. Phys. J. A* **1**, 151 (1998)
[16] C O Dorso and J Aichelin, *Phys. Lett. B* **345**, 197 (1995)
[17] R K Puri and J Aichelin, *J. Comput. Phys.* **162**, 245 (2000)
[18] R K Puri *et al*, *Phys. Rev. C* **54**, R28 (1996)
[19] Y K Vermani and R K Puri, *Europhys. Lett.* **85**, 62001 (2009)
[20] Y K Vermani and R K Puri, *Cent. Eur. J. Phys.* **9**, 621 (2010)
[21] Y K Vermani, J K Dhawan, S Goyal, R K Puri and J Aichelin, *J. Phys. G* **37**, 015105 (2010)
S Goyal and R K Puri, *Phys. Rev. C* **83**, 047601 (2011)
[22] J Y Liu *et al*, *Phys. Rev. Lett.* **86**, 975 (2001)
J Y Liu *et al*, *Phys. Rev. C* **63**, 054612 (2001)
[23] J Y Liu, Q Zhao, S J Wang, W Zuo and W J Guo, *Nucl. Phys. A* **687**, 475 (2001)
[24] B A Li, C M Ko and Z Z Ren, *Phys. Rev. Lett.* **78**, 1644 (1997)
[25] Y M Zheng, C M Ko, B A Li and B Zhang, *Phys. Rev. Lett.* **83**, 2534 (1999)
[26] R Pak *et al*, *Phys. Rev. Lett.* **78**, 1026 (1997)
[27] F S Zhang, B A Bian and H Y Zhou, *Int. J. Mod. Phys. E* **17**, 1865 (2008)
[28] F Gagnon-Moisan, M-F Rivet, B Borderie, R Roy and the INDRA Collaboration, *Proceedings of International Workshop on Multifragmentation and Related Topics* (Catania, Italy, 2009) p. 165
[29] A Jain, S Kumar and R K Puri, *Phys. Rev. C* **85**, 064608 (2012)
[30] S Kaur and R K Puri, *Phys. Rev. C* **87**, 014620 (2013)
S Kaur and R K Puri, *Phys. Rev. C* **90**, 037602 (2014)
S Kaur and R K Puri, *Phys. Rev. C* **89**, 057603 (2014)
[31] P Russotto *et al*, *Phys. Rev. C* **81**, 064605 (2010)
[32] Y Zhang, Z Li, C Zhou and M B Tsang, *Phys. Rev. C* **85**, 051602(R) (2012)
[33] W D Myers and W J Swiatecki, *Nucl. Phys. A* **336**, 267 (1980)
W D Myers and K H Schmidt, *Nucl. Phys. A* **410**, 61 (1983)
[34] D Klakow, G Welke and W Bauer, *Phys. Rev. C* **48**, 1982 (1993)
T Alm, G Röpke, W. Bauer, F Daffin and M Schmidt, *Nucl. Phys. A* **587**, 815 (1995)
[35] S Gautam, A D Sood, R K Puri and J Aichelin, *Phys. Rev. C* **83**, 034606 (2011)
S Gautam, R Kumari and R K Puri, *Phys. Rev. C* **86**, 034607 (2012)
[36] S Gautam *et al*, *Phys. Rev. C* **83**, 014603 (2010)
S Gautam, R Chugh, A D Sood, R K Puri, Ch Hartnack and J Aichelin, *J. Phys. G* **37**, 085102 (2010)
[37] S Kumar, Rajni and S Kumar, *Phys. Rev. C* **82**, 024610 (2010)
[38] H Kruse, B V Jacak, J J Molitoris, G D Westfall and H Stöcker, *Phys. Rev. C* **31**, 1770 (1985)
J Singh and R K Puri, *J. Phys. G* **27**, 2091 (2001)
[39] C Dorso and J Randrup, *Phys. Lett. B* **301**, 328 (1993)
[40] R K Puri, J Singh and S Kumar, *Pramana – J. Phys.* **59**, 19 (2002)